Gd^{3+} ions doping effect on the microstructure and electrical properties of $Mn_{0.9}Zn_{0.1}Ni_{0.05}Ti_{0.05}Gd_tFe_{1.9-t}O_4$ ferrite

Ahmed Abo Arais

Department of Physics and Engineering Mathematics, Faculty of Electronic Engineering, Menoufia University, Menouf, Egypt.

Abstract- Samples of the general chemical formula $Mn_{0.9}Zn_{0.1}Ni_{0.05}Ti_{0.05}Gd_tFe_{1.9-t}O_4$; ($0.0 \le t \le 0.05$; step 0.01) were prepared using the standard ceramic method**.** XRD analysis reveals that the samples have a cubic spinel single phase structure for $0.0 \le x \le 0.02$ while for $x \ge 0.03$ a small peak of secondary phase appears and becomes more remarkable with increasing Gd^{3+} ions content. The experimental parameter constant ($\mathbf{a}_{exp}$) initially increases and then decreases with increasing Gd content (t) which may be attributed to the differences in the ionic radii of the cations involved and the solubility limit of Gd^{3+} ions. The cation distribution of the prepared samples was assumed and the theoretical lattice parameter was also calculated and compared with the experimental one. DC electrical resistivity (ρ) was measured as a function of temperature using the two probe method. The substitution of Fe^{3+} ions by Gd^{3+} ions improves the physical properties by increasing resistivity and consequently decreasing the dielectric loss which reduces the occurrence of eddy currents so, they can be used in telecommunications, memory cores and transformers. The temperature variation of resistivity exhibits two breaks, each break refers to a change in the activation energy. The Curie temperature (T_c) estimated from DC resistivity measurements decreases with increasing Gd^{3+} ions.

Keywords: Rare earth ions; ferrites; microstructure; dc resistivity;

1. Introduction

Ferrites are ferrimagnetic materials which possess the combined properties of magnetic materials and insulators. In soft ferrites, greater resistivity reduces the occurrence of eddy currents which are caused by rapidly fluctuating magnetic fields and results in the loss of signal energy to heat. As a consequence of their reduction of eddy currents, they can be used in telecommunications, memory cores and transformers especially at higher frequencies [1].

Mn-Zn ferrites represent an important class of soft ferromagnetic materials characterized by high magnetic permeability and relative low magnetic losses. Thus, they are mainly used as the cores for inductors, recording heads and in switch mode power supplies. Ferrites serve as better Electromagnetic interference (EMI)

suppressors compared to their dielectric counterparts on account of their excellent magnetic properties, broad band electronic circuit transformers, integrated services digital network (ISDN), local area network (LAN), wide area network (WAN), pulse transformer, and background lighting, etc [2].

By adding a small amount of foreign ions, an excellent modification in the structure, magnetic and electric properties would be obtained. Several cations such as Zn^{2+}, Co^{2+}, Ni^{2+} and Ti^{4+} ions have been attempted by several researchers in order to improve the electrical and magnetic properties of manganese ferrites [3-9]. Ti^{4+} ions substitution at the iron site in manganese ferrites is known to be effective in reducing magneto-crystalline anisotropy and enhancing the electrical resistivity, these properties are suitable for a wide range of industrial applications. Ni^{2+} ions are also selected with Ti^{4+} ions to maintain the overall neutrality in the material [10].

Rare earth ions can be divided into two categories [5]: the first one in which R^{3+} ions with radius very close to the Fe^{3+} ions can enter into the spinel lattice, while the second type of R^{3+} ions has an ionic radius larger than Fe^{3+} ions. During the sintering process, some of these ions will diffuse to the grain boundaries and form an isolating ultra-thin layer around the grains, contributing to the formation of secondary phases [11].

In this work, we study the effect of Gd^{3+} ions substitution on the microstructure and electric properties of $Mn_{0.9}Zn_{0.1}Ni_{0.05}Ti_{0.05}Gd_tFe_{1.9-t}O_4$ ($0.0 \leq t \leq 0.05$, with step 0.01) to get the desired concentration of Gd^{3+} ions to obtain high electric properties to reduce the eddy currents and consequently the energy losses to open new era of applications in telecommunications and electronics.

2. Experimental

Samples $Mn_{0.9}Zn_{0.1}Ni_{0.05}Ti_{0.05}Gd_tFe_{1.9-t}O_4$ ($0.0 \leq t \leq 0.05$, with step 0.01) were prepared by the standard ceramic

technique. The structure of the prepared samples was identified using XRD on a Brucker axis D8 diffractometer of Cu-K_α radiation (λ =1.5418 Å). The porosity percentage (P %) was calculated from the relation, [$P = (1-D_b/D_x)$]. The two surfaces of each pellet were coated with silver paste and checked for good electrical contact. The dc resistivity of the prepared samples was measured as a function of temperature using the two-probe method as a function of temperature.

3. Results and discussion

3.1. Structural properties

The XRD patterns of $Mn_{0.9}Zn_{0.1}Ni_{0.05}Ti_{0.05}Gd_tFe_{1.9-t}O_4$ ($0.0 \leq t \leq 0.05$, step 0.01) indicate that the samples reveal a single phase cubic spinel structure as shown in Fig. (1).The crystallographic planes of the main characteristic peaks of cubic spinel structure that perfectly matched with the theoretical data of Franklinite spinel structure (card: No. 74-2402). No extra lines which indicate the existence of secondary phases.

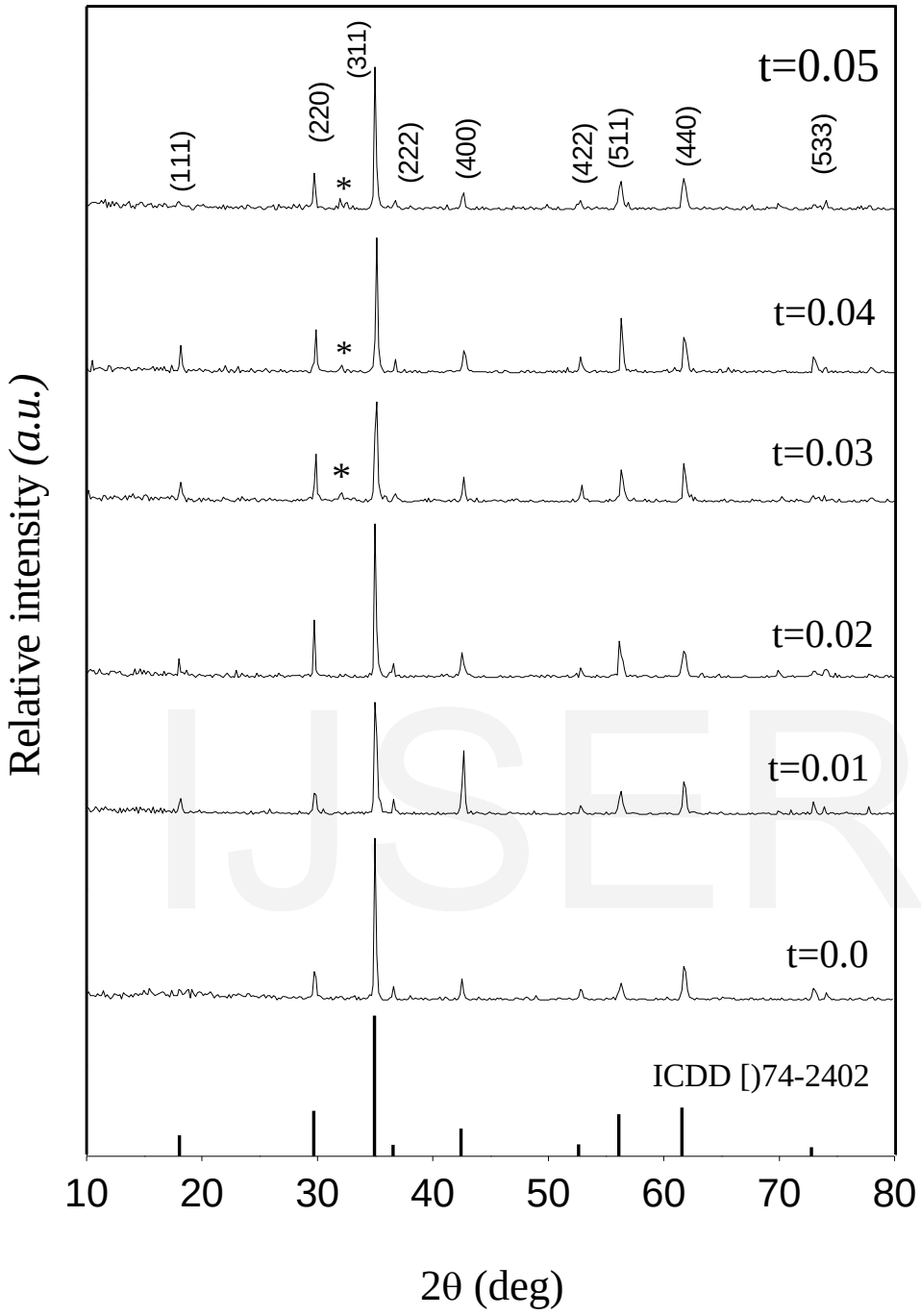

Fig. (1): X-ray diffraction patterns for the prepared samples. $Mn_{0.9}Zn_{0.1}Ni_{0.05}Ti_{0.05}Gd_tFe_{1.9-t}O_4$ ($0.0 \le t \le 0.05$, step 0.01)

Figure (2) shows that the positions of peaks were shifted to a higher value of 2θ with substitution of Gd^{3+} ions, indicating that the lattice parameter for the samples changes with Gd-content (t). Figure (3) shows that as Gd content (t) increases the porosity decreases. It is well known that the porosity of ceramic samples results from two sources namely intragranular porosity (P_{intra}) and intergranular porosity (P_{inter}), so that the total percentage porosity (P%) could be calculated as the sum of two types. The total percentage of porosity of all the samples can be measured [16]. X-ray density which is dependent on molecular weight and lattice constant of the samples and the bulk density are increasing with increasing Gd content (t). The large values of X-ray density than bulk density may be due to the existence of pores in the samples. Since the formation of secondary phase ($Gd_3Fe_5O_{12}$) fills inter-granular voids and exhibit good densification, a decrease in porosity was expected with Gd substitution [17].

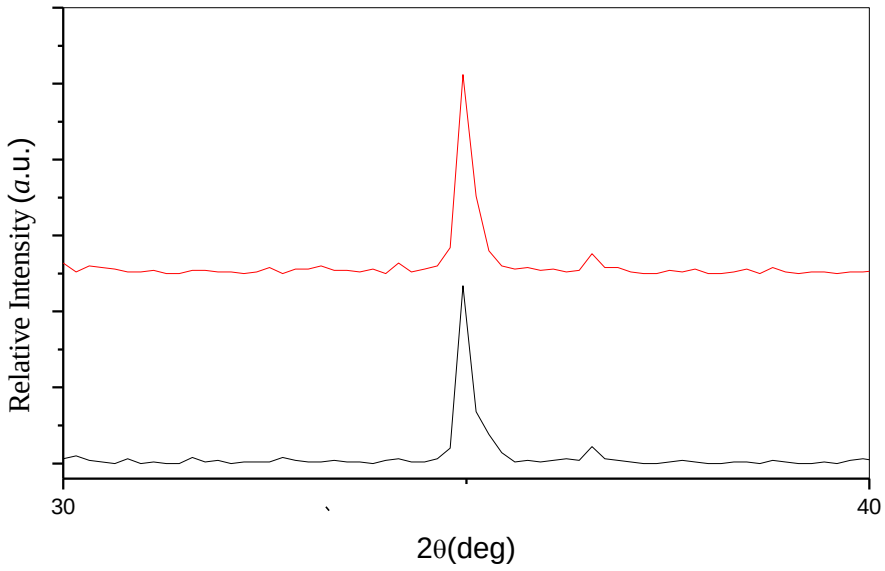

Fig. (2)**:** Effect of Gd concentration on the XRD peaks

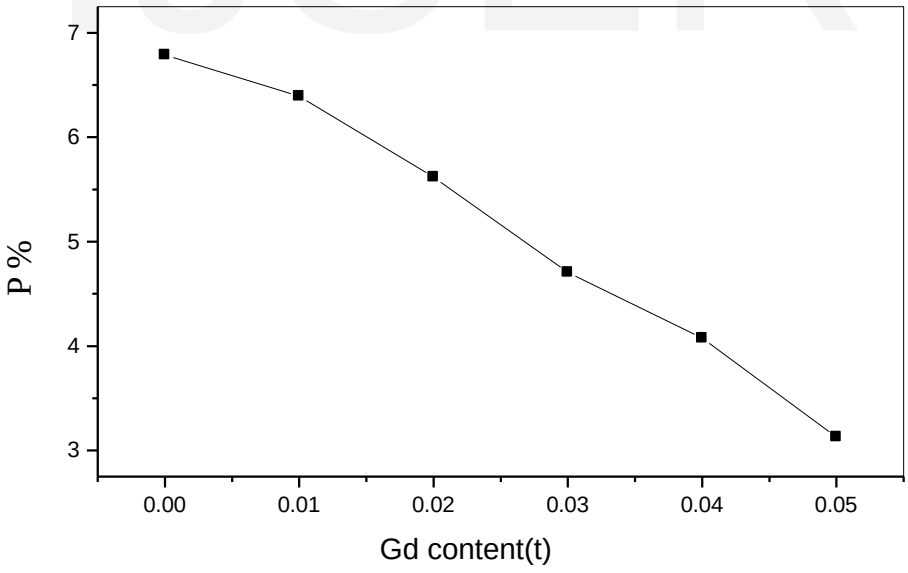

Fig. (3): Variation of the percentage porosity (P%) as a function of Gd content (t).

The experimental lattice parameter of the prepared samples was calculated and plotted as a function of Gd^{3+} ion content (t) which gradually increases up to t = 0.02, while for higher Gd concentration (t) it decreases. The gradual increase in the experimental lattice parameter (a_{exp}) with the increase of Gd^{3+} ions concentration (t) can be explained on the basis of relative ionic radii of Gd^{3+} and Fe^{3+} ions. Since the Gd^{3+} ion has a larger ionic radius (0.97 Å) than that of the Fe^{3+} ion (0.645 Å), a partial replacement of the Fe^{3+} ion by Gd^{3+} ion causes an expansion of the spinel lattice, leading to an increase in the lattice constant which obeys Vegard's law [15]. For $0.03 \leq t \leq 0.05$, there is a decrease in the experimental lattice parameter (a_{exp}) which can be attributed to the existence of a solubility limit for Gd ions at t = 0.02. Once the solubility limit is reached, the Gd^{3+} ion could no longer dissolve in the spinel lattice but rather diffuse to the grain boundaries combining with Fe^{3+} ion to form ($Gd_3Fe_5O_{12}$) and forming an ultra thin layer around grains [18]. The correlation between the ionic radii and the theoretical lattice parameter (a_{th}) is calculated using the following equation.

$$a_{th} = \frac{8}{3\sqrt{3}}[(r_A + R_o) + \sqrt{3}(r_B + R_o)]$$

where R_o is the radius of the oxygen ion (1.38 Å), r_A and r_B are the ionic radii of tetrahedral A- and octahedral B-site, respectively. In order to calculate r_A and r_B it is necessary to know the cation distribution for the given system. In general, Zn^{2+} ion has higher preference for (A-site), Ti^{4+}, Ni^{2+} and Gd^{3+} ions have higher preference for B-site while Fe^{3+} and Mn^{2+} ions are distributed between the tetrahedral A- and octahedral B-sites. The postulated cation distribution can be written as:

$$(Zn_{0.1}^{2+} Mn_{0.7}^{2+} Fe_{0.2}^{3+})[Mn_{0.2}^{2+} Ni_{0.05}^{2+} Ti_{0.05}^{4+} Gd_t^{3+} Fe_{1.7-t}^{3+}] O_4^{2-}$$

where the brackets ( ) and [ ] denote to A- and B- sites respectively. The ionic radius of each site was calculated according to the following equations.

$r_A = [(0.1)\, r_{Zn^{2+}} + (0.7)\, r_{Mn^{2+}} + (0.2)\, r_{Fe^{3+}}]$

r_B= 0.5 [(0.2) $r_{Mn^{2+}}$ + (0.05) $r_{Ni^{2+}}$ + (0.05) $r_{Ti^{4+}}$ + (t) $r_{Gd^{3+}}$ +(1.7-t) $r_{Fe^{3+}}$]

where $r_{Zn^{2+}}$,$r_{Mn^{2+}}$, $r_{Ni^{2+}}$, $r_{Ti^{4+}}$, $r_{Gd^{3+}}$and $r_{Fe^{3+}}$ are the ionic radii of Zn^{2+}, Mn^{2+}, Ni^{2+}, Ti^{4+} ,Gd^{3+} and Fe^{3+} ions respectively. The theoretical and experimental values of lattice parameter are plotted against Gd-content (t) in Fig. (4). One could note that the theoretical lattice parameter (a_{th}) increases slightly with increasing Gd content (t) according to the assumed cation distribution. Figure (4) shows also that the experimental lattice parameter is greater than the theoretical one, which can be attributed to the formation of Fe^{2+} ion of larger ionic radius during the sintering process.

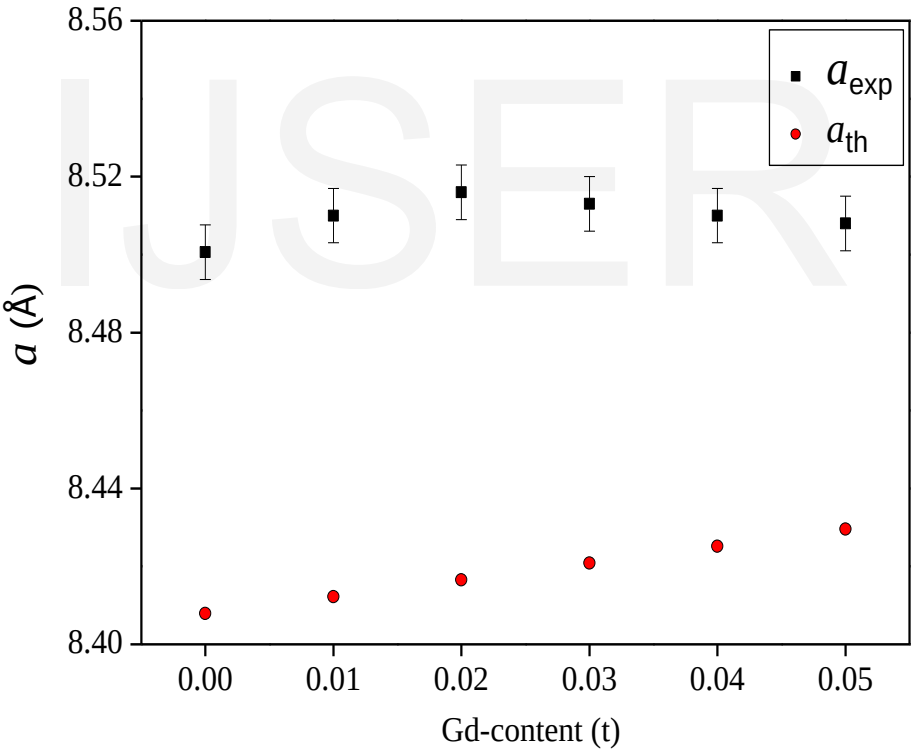

Fig. (4): Variation of theoretical (a_{th}) and experimental (a_{exp}) lattice parameter as a function of Gd content (t).

3.2 Electrical Properties

The dc electric resistivity of the spinel system $Mn_{0.9}Zn_{0.1}Ni_{0.05}Ti_{0.05}Gd_tFe_{1.9-t}O_4$ ($0.0 \le t \le 0.05$, step 0.01) was studied as a function of absolute temperature over a wide temperature range from room temperature up 650 K. Figure (5) shows the variation of resistivity, expressed as ($\ln \rho_{dc}$) with (1000/T) for all the studied samples. Figure (6) shows the variation between ($\ln \rho_{dc}$) and (1000/T) for sample $Mn_{0.9}Zn_{0.1}Ni_{0.05}Ti_{0.05}Gd_{0.04}Fe_{1.86}O_4$, as an example of the studied samples to illustrate the transition temperatures. The temperature dependence of resistivity exhibits two breaks and three distinct regions (I, II and III). Such a break was associated with a change in the slope that can be either linked with magnetic ordering and with a change in the conduction mechanism. The first region is attributed to extrinsic conduction mechanism due to the existing impurities; it extends from room temperature up to the first transition temperature (T_1) for all studied samples. The second transition temperature ($T_{C\ elec.}$) is always attributed to the magnetic phase transition from ferrimagnetic to paramagnetic state and shown in Table [1], which ranged from 470 to 554 K for all samples and agrees with the previously published data for spinel ferrites. The activation energies ($E_{ferri.}$) for region II and ($E_{para.}$) for region III were calculated from the slopes of the curve in Fig. (6). It is observed that ($E_{para.}$) is greater than ($E_{ferri.}$) for all investigated samples as reported in Table [1]. The increase of the activation energy from order to disorder state may be attributed to the volume expansion above ($T_{C\ elec.}$) due to increasing the jumping length of the charge carriers. Increasing temperature leads to decrease in resistivity, which helps the trapped charges to be liberated and contribute in the conduction process, causing a decrease in the resistivity. This decrease could be also related to the increase in the drift mobility of the thermally activated electrons according to the hopping conduction mechanism. The electrical resistivity was found to increase gradually with increasing Gd content (t) from 8.8×10^3 Ω.m to 19.2×10^3 Ω.m, the increase of the resistivity with

Gd^{3+} ions concentration can be explained according to that the Gd^{3+} ions reside on B-site hence Gd^{3+} ions will impede the electron exchange between Fe^{2+} and Fe^{3+} ions on B-sites. In addition for higher Gd^{3+} ion substitution i.e. at $0.03 \leq t \leq 0.05$, the resistivity also increases, this can be attributed to that Gd^{3+} ions enter partially into the lattice sites and the rest may reside at the grain boundary creating a secondary phase ($Gd_3Fe_5O_{12}$) as a large number of insulating grains boundaries surrounded spinel ferrite which oppose the electron flow [19]. The increase of the electrical resistivity for the investigated system reduces the occurrence of the eddy currents and consequently reduces the energy loss as heat. Accordingly they can be used in many applications such as transformer cores and memory cores. Similar results were obtained for Co-Ferrite [20].

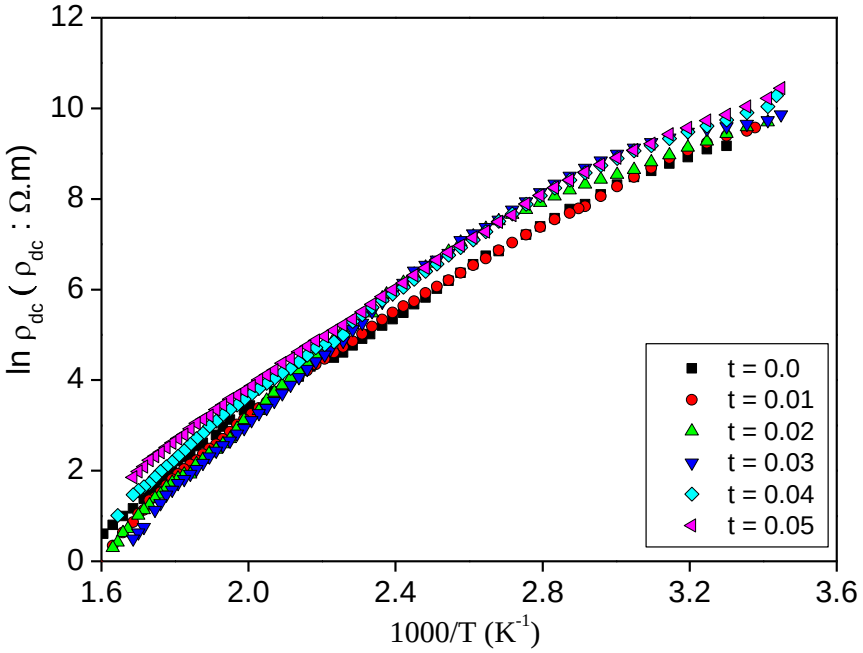

Fig. (5): Relation between resistivity and temperature of $Mn_{0.9}Zn_{0.1}Ni_{0.05}Ti_{0.05}Gd_tFe_{1.9-t}O_4$, $(0.0 \leq t \leq 0.05)$.

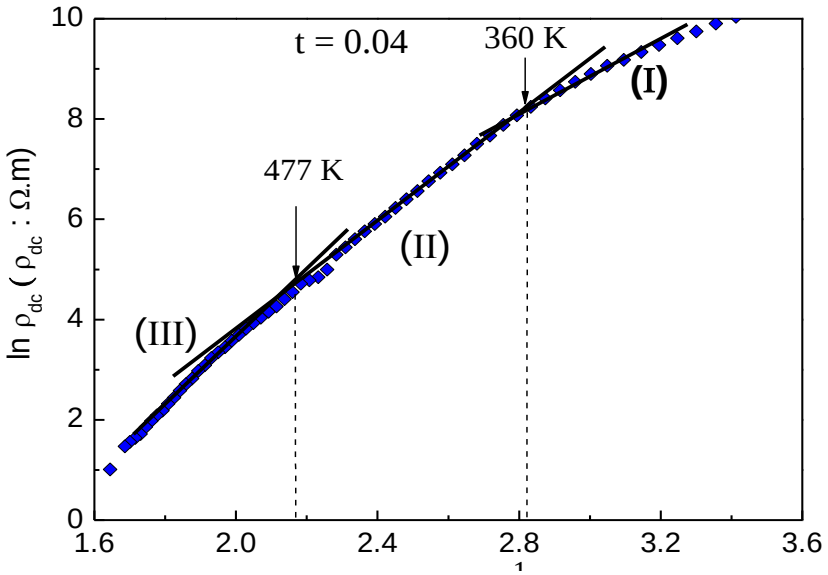

Fig. (6): Relation between resistivity and temperature for the sample of t = 0.04 as an example.

Table [1]: Effect of Gd-content (t) on the calculated values of activation energies, the transition temperatures and the room temperature resistivity.

t	$E_{ferri.}$(eV)II	$E_{para.}$(eV)III	T_1(K)	$T_{C.}$(K)
0.0	0.42	0.67	353	558
0.01	0.47	0.59	383	498
0.02	0.54	0.64	380	489
0.03	0.53	0.59	358	482
0.04	0.48	0.63	360	477
0.05	0.47	0.60	358	470

References

[1] M.A. Ahmed, S.T. Bishay, Thermal studies of the electrical conductivity of LiCoYb-ferrites, Journal of Physics and Chemistry of Solids 64 (2003) 769–775.

[2] G. Ott, J. Wrba, R. Lucke, Recent developments of Mn–Zn ferrites for high permeability applications, J. Magn. Magn. Mater. 254-255(2003)535-537.

[3] A. .Dogra, M. Singh, V.V. Siva Kumar, N. Kumar and R. Kumar, Irradiation effect on dielectric properties of $NiMn_{0.05}Ti_x(Zn,Mg)xFe_{1.95-2x}O_4$ ferrite thin films, Nucl. Instrum. Meth. Phys. B212 (2003) 184.

[4] S. Kumar, R. Kumar, S.K. Sharma, V.R. Reddy, A. Banerjee and Alimuddin, Temperature-dependent Mössbauer and dielectric studies of $Mg_{0.95}Mn_{0.05}Fe_{1.0}Ti_{1.0}O_4$, J. Solid State Commun. 141 (2007)706–709.

[5] D.S. Birajdar, D.R. Mane, S.S. More, V.B. Kawade and K.M. Jadhav, Structural and Magnetic Properties of $Zn_xCu_{1.4-x}Mn_{0.4}Fe_{1.2}O_4$ Ferities, J. Mater. Lett. 59 (2005) 2981–2985.

[6] L. Nalbandian, A. Delimitis, V.T. Zaspalis, E.A. Deliyanni, D.N. Bakoyannakis and E.N. Peleka, Hydrothermally prepared nanocrystalline Mn-Zn ferrites: Synthesis and characterization , J. Micropor. Mesopor. Mater. 114 (2008) 465–473.

[7] M.K. Shobanaa, S. Sankara and V. Rajendranb, Characterization of $Co_{0.5}Mn_{0.5}Fe_2O_4$ nanoparticles, Mater. Chem. Phys. 113 (2009)10–13.

[8] A.M.M. Farea, S. Kumar, K.M. Batoo, A. Yousef, C.G. Lee and Alimuddin, Influence of the doping of Ti^{4+} ions on the electrical and magnetic properties of $Mn_{1+x}Fe_{2-2x}Ti_xO_4$ ferrite, J. Alloy Compd. 469 (2009)451–457.

[9] M.P. Horvath, Microwave applications of soft ferrites, J. Magn. Magn. Mater. 215–216 (2000)171–183.

[10] M.N. Ashiq, N. Bibi and M.A. Malana, Effect of Sn–Ni substitution on the structural, electrical and magnetic properties of mixed spinel ferrites, J. Alloy Compd. 490 (2010)594–597

[11] M.A. Ahmed, E. Ateia, S.I. El-Dek, Spectroscopic analysis of ferrite doped with different rare earth elements, Vibrational Spectroscopy 30 (2002) 69-75.

[12] P.K. Roy and J. Bera, Materials Res. Bull. 42 (2007) 77–83.

[13] S.S.R. Inbanathan, V. Vaithyanathan, J. Arout Chelvane, G. Markandeyulu and K. Kamala Bharathi, J. Magn. Magn. Mater. 353 (2014) 41–46.

[14] N. Rezlescu, E. Rezlescu, C. Pasnicu and M.L. Craus, J. Phys.: Condens. Matter. 6 (1994) 5707–5716.

[15] R. Islam, M.A. Hakim, M.O. Rahman, H. Narayan Das and M.A. Mamun, J. Alloy Compd. 559 (2013) 174–180.

[16] J. Jing, L. Liangchao and X. Feng, J. Rare Earths 25 (2007) 79–83.

[17] N. Rezlescu, E. Rezlescu, P.D. Popa and L. rezlescu, J. Alloy. Comp. 275–277 (1998) 657–659.

[18] E.E. Sileo and S.E. Jacobo, J . Phy . B 354 (2004) 241.

[19] N. Rezlescu, E. Rezlescu, C. Pasnicu and M.L. Craus, J. Magn. Magn. Mater. 136 (1994) 319–326.

[20] M.T. Rahman and C.V. Ramana, Cerama. Inter. 40(9),1433,2014.